Electronic Supplementary Information (ESI)

Solvent-induced structural transformation in a one-dimensional coordination polymer

Kangwoo Jin,[a] Nohyoon Park,[a] Yongdeok Ahn,[a] Daeha Seo,[a] Dohyun Moon,*[b] Jooyoung Sung,*[a] and Jinhee Park*[a]

[a] Department of Physics and Chemistry, Daegu-Gyeongbuk Institute of Science and Technology, Daegu 42988, Republic of Korea. Email: jooyoung@dgist.ac.kr; jinhee@dgist.ac.kr
[b] Beamline Department, Pohang Accelerator Laboratory
Pohang 37673, Republic of Korea. Email: dmoon@postech.ac.kr

Table of Contents

Part S1. Materials and Instrumentation

Materials

1,8-Naphthalic anhydride (97%), 5-aminoisophthalic acid (95%), triethyl amine (99%), *N,N*-dimethylformamide (DMF, 99.8%), and zinc acetate dihydrate ($Zn(OAc)_2 \cdot 2H_2O$, 97%) were purchased from Alfa Aesar. Deuterium oxide (D_2O, 99.9%) was purchased from Sigma Aldrich. Methanol (MeOH, 99.99%) was purchased from B&J. Dimethyl sulfoxide (DMSO, 99.5%), dichloromethane (DCM, 99.5%), sodium hydroxide beads (NaOH, 98%) and anhydrous ethanol (EtOH, 99.5%) were purchased from Daejung Chemical. All commercial chemicals were used without further purification.

Instrumentation

Proton nuclear magnetic resonance (^{1}H-NMR) spectrum was measured on the Fourier transform nuclear magnetic resonance spectrometer from AVANCE III 400 (Bruker). Chemical shifts are reported in ppm downfield referenced against DMSO-d_6 (δ = 2.50) and D_2O (δ = 4.80). Field emission-scanning electron microscopy (FE-SEM) and was collected through SU8020 from Hitachi. Ltd. Powder X-ray diffraction (PXRD) data were obtained by the Empyrean X-ray diffractometer (Panalytical) with Ni-filtered Cu Kα radiation ($\lambda_{K\alpha1}$ = 1.541 Å, 40 kV, and 30 mA). Inductively coupled plasma optical emission (ICP-OES) data were obtained using iCAP7400DUO (Thermo Scientific). Emission spectra were recorded at room temperature with Synergy H1 (Biotek). Gas sorption isotherms were collected by the Brunauer-Emmett-Teller (BET) analyzer from Soletek (BELSORP-max) and Micromeritics Instrument Corporation (3-flex). UV-Vis spectra were obtained on a SHIMADZU spectrometer (UV-2600). Fluorescence and fluorescence excitation spectra were taken with F7000 (Hitachi). Fourier transform-infrared (FT-IR) spectra were collected by Nicolet Continuum (Thermo Scientific) with attenuated total reflectance mode. Samdri-PVT-3D was used for CO_2 supercritical point drying (CPD). Thermogravimetric analysis (TGA) data were obtained by Auto Q500 (TA instruments) with a heating rate of 2 °C/min to 300 °C and 10 °C/min to 1000 °C. Elemental analysis (EA) was performed on Elementar (Vario MICRI Cube). Optical microscopy experiments were performed using an inverted microscope (Nikon, ECLPSE Ti2-E) equipped with a perfect focus system (PFS, TI2-N-ND-P), a motorized stage (TI2-S-SE-E), and electron multiplying charge-coupled device (EM CCD, Andor, iXorn Ultra 897). LED lamp (Nikon, TI2-D-LHLED) and mercury lamp (Nikon, intensilight C-HFGI) were used as a light source for bright-field and Epi-fluorescence/dark field microscope, respectively. The fluorescence images were acquired using an ellipsoidal dot mirror installed at a filter cube set (DAPI, FITC, and mCherry HQ filter set). A 20× objective lens (Nikon, CFI Plan Apochromat, N.A. 0.75) was used for MOF crystal imaging. The fluorescence images were acquired using Nikon NIS-Elements advanced research software and analyzed with ImageJ software (http://imagej.nih.gov/ij/download.html).

Picosecond time-resolved fluorescence decay

Time-resolved fluorescence lifetime experiments were conducted using the time-correlated single-photon-counting (TCSPC) technique. We employed a tunable excitation laser source that generated pulses of ~ 100 fs from a mode-locked Ti:sapphire laser (Spectra-Physics, Mai Tai BB) operating at a repetition rate of 800 kHz via a homebuilt pulse-picker. Specifically, the laser pulse output at 760 nm was frequency-doubled by a 1 mm thickness of a second harmonic crystal (β-barium borate, BBO, Type-I, θ =29.2°, EKSMA), resulting in a 380 nm pulse used for sample excitation. The emitted fluorescence from samples was collected and amplified by a microchannel plate photomultiplier (MCP-PMT, Hamamatsu, R3809U-51) with an integrated thermoelectric cooler (Hamamatsu, C4878), all connected to a TCSPC board (Becker&Hickel SPC-130). The overall instrumental response function exhibited a full width at half maximum (FWHM) of approximately 25 ps. To excite the samples, a vertically polarized pump pulse, regulated by a Glan-laser polarizer was utilized. Simultaneously, in the fluorescence collection path, a sheet polarizer was positioned at an angle complementary to the magic angle (54.7°) to ensure polarization-independent measurements of fluorescence decays.

For time-resolved fluoresce decay measurements, the 1D-acetone (2%) and DMSO (spectroscopic grade solvents, Sigma-Aldrich) were placed in a 2 mm quartz cuvette. We allowed sufficient time for sample to dissipate in order to ensure the sample concentration remained constant throughout the measurement. Additionally, we measured the fluorescence

intensity profiles and absorption spectra of samples both before and after the TCSPC measurements to monitor any potential sample degradation due to the irradiation. However, no noticeable spectroscopic changes were observed.

Part S2. Syntheses

1. Synthesis of H_2**L**

H_2**L** was synthesized according to the previously reported procedure.[1]

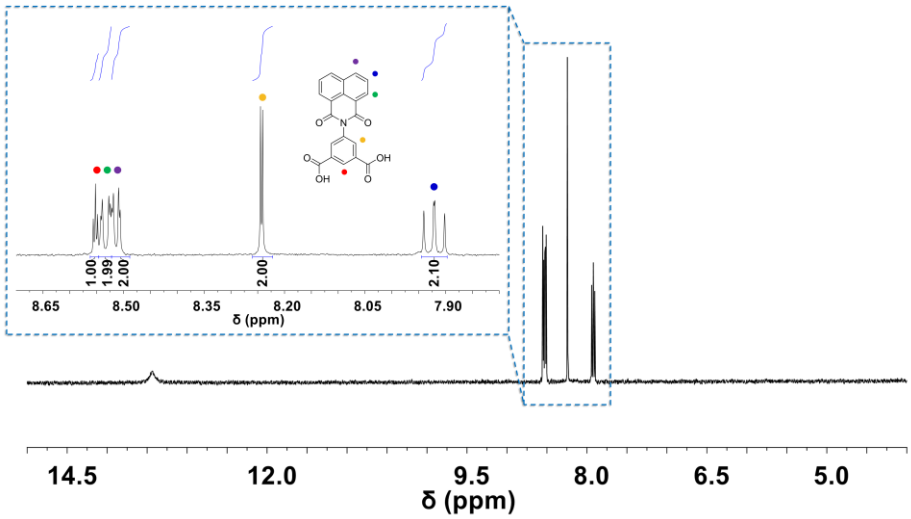

Fig. S1 NMR spectrum of H_2**L** in DMSO-d_6.

2. Synthesis of 1D-DGIST-18

H_2**L** (500 mg, 1.38 mmol) was dissolved in 100 mL of DMSO and added to the $Zn(OAc)_2{\cdot}2H_2O$ (303.8 mg, 1.38 mmol), dissolved in 100 mL of DMSO in a 250 mL lab bottle. The lab bottle stood at room temperature (20-25°C) for a day. Colorless polyhedral crystals of 1D-DGIST-18 were obtained (0.5492 g and 93.5% yield).

For gas sorption experiments, 1D-DGIST-18 was washed with DMSO several times and further exchanged with acetone. Soxhlet extraction was performed using either acetone at 100 °C, EtOH, or MeOH at 140 °C, with each extraction lasting for 12 hours. Subsequently, the samples were either subjected to CPD or degassed under vacuum at 80 °C for 12 hours. After the CPD process, the samples were further degassed under vacuum at room temperature for an additional 12 hours. During the CPD process, a stasis mode was employed to allow for adequate CO_2 exchange, based on methods reported in earlier literature.[2]

Elemental analysis of activated 1D-DGIST-18. Calc. (%): C, 56.58; H, 2.12; N, 3.30; Zn, 15.40. Found (%): C, 56.57; H, 2.14; N, 3.30; Zn, 14.40 (Zn from ICP-OES analysis).

3. Synthesis of 3D-DGIST-18

A solid mixture of H_2**L** (500 mg, 1.38 mmol) and $Zn(OAc)_2{\cdot}2H_2O$ (303.8 mg, 1.38 mmol) was placed in 200 mL of DMF in a Teflon lined 250 mL lab bottle. The solution was sonicated for 30 min and heated at 120 °C. Sufficient reaction time was required because of the poor solubility of H_2**L** in DMF. After 7 days, polyhedral crystals of 3D-DGIST-18 were obtained (0.5346 g and 91.2% yield).

Elemental analysis of activated 3D-DGIST-18. Calc. (%): C, 56.58; H, 2.12; N 3.30; Zn, 15.40. Found (%): C, 58.39; H, 3.80; N, 4.96; Zn, 15.79 (Zn from ICP-OES analysis)

Part S3. Crystallographic Information

1. Single Crystal X-ray crystallography (SCXRD)

The 1D-DGIST-18, 1D-DGIST-18', and 3D-DGIST-18 crystals were coated with Parabar 10312 (Hampton Research Inc.) to be mounted on a micro-loop, and transferred to a cold stream of liquid nitrogen (100 – 253 K). The single-crystal X-ray diffraction data collection was carried out using a synchrotron-based X-ray source produced from a PLSII 2D bending magnet with a Si(111) double crystal monochromator and Rayonix MX225HS CCD area detector. The PAL BL2D-SMDC program[3] was used for one set of data collection at the following conditions: detector distance of 66 mm, 1-axis omega scan with $\Delta\omega$ of 1° and the exposure time of 0.3 – 1sec/frame. HKL3000sm (ver. 717.6)[4] was used for cell refinement, reduction, and absorption correction. The structures were solved by the intrinsic phasing method using SHELXT-2018/2[5] and refined by full matrix least-squares on F^2 using SHELXL-2019/3[6]. All non-hydrogen atoms were refined anisotropically, and all H atoms were placed in geometrically idealized positions and constrained to ride on their parent atoms with C–H = 0.94 – 0.98 Å and with U_{iso}(H) values of 1.2 and 1.5 U_{eq} of the parent atoms. For 1D-DGIST-18', and 3D-DGIST-18, the final refinements were performed with modified structural factors based on the SQUEEZE routine of PLATON[7] to remove diffused electron densities from disordered structural solvents. For 1D-DGIST-18', the electron count in an empty cell, as measured by SCXRD, was found to be 164, which corresponds to approximately 5 Acetone molecules in S.A.V. For 3D-DGIST-18, the electron count in an empty cell, as measured by SCXRD, was found to be 229, which corresponds to approximately 6 DMF molecules in S.A.V. Some SHELXL restraints, such as DFIX, DANG, SIMU, DELU, and RIGU, were used to correct the geometry of the disordered parts and the thermal parameters of the corresponding atoms. The summary of crystallographic data and refinement parameters are listed in Table S1. Further details may be obtained from the Cambridge Crystallographic Data Centre at https://www.ccdc.cam.ac.uk/deposit. CCDC entries 2303707 – 2303709 contain the supplementary crystallographic data for this article.

Table S1. Crystal structure refinement data for 1D-DGIST-18, 1D-DGIST-18′, and 3D-DGIST-18.

Identification code	1D-DGIST-18	1D-DGIST-18′	3D-DGIST-18
CCDC #	2303707	2303708	2303709
Empirical formula	C_{30} H_{39} N O_{11} S_5 Zn	C_{22} H_{17} N O_8 S Zn	C_{49} H_{39} N_5 O_{15} Zn_2
Formula weight	815.29	520.79	1068.59
Temperature (K)	100(2)	100(2)	253(2)
Wavelength	0.700	0.700	0.700
Crystal system	*Monoclinic*	*Monoclinic*	*Monoclinic*
Space group	*P2₁/c*	*P2₁/c*	*Cc*
Unit cell dimensions	*a* = 12.558(3) Å	*a* = 8.5630(17) Å	*a* = 18.659(4) Å
	b = 16.386(3) Å	*b* = 16.995(3) Å	*b* = 19.486(4) Å
	c = 18.212(4) Å	*c* = 17.633(4) Å	*c* = 17.039(3) Å
	α = 90°	α = 90°	α = 90°
	β = 103.90(3)°	β = 101.24(3)°	β = 122.41(3)°
	γ = 90°	γ = 90°	γ = 90°
Volume (Å^3)	3637.9(13)	2516.9(9)	5230(2)
Z	4	4	4
$d_{calc.}$ (g/cm^3)	1.489	1.374	1.357
Absorption coefficient (mm^{-1})	0.972	1.056	0.946
F(000)	1696	1064	2192
Crystal size (mm^3)	0.340 x 0.300 x 0.160	0.029 x 0.025 x 0.018	0.241 x 0.044 x 0.036
Theta range for data collection	1.645 to 25.999	1.655 to 25.994	1.637 to 27.000
Index ranges	-15<=h<=15	-10<=h<=10	-23<=h<=23
	-19<=k<=19	-19<=k<=19	-25<=k<=25
	-22<=l<=22	-22<=l<=22	-22<=l<=22
Collected reflections	27361	18357	22012
Independent reflections	7239 [R(int) = 0.0375]	4885 [R(int) = 0.1151]	11875 [R(int) = 0.0542]
Completeness	97.1 %	94.8 %	99.5
Data / restraints / parameters	7239 / 96 / 511	4885 / 228 / 314	11875 / 164 / 705
Goodness-of-fit on F^2	1.072	1.185	1.044
Final R indices [*I*>2sigma(*I*)]	R1 = 0.0574, wR2 = 0.1624	R1 = 0.1148, wR2 = 0.3481	R1 = 0.0387, wR2 = 0.1059
R indices (all data)	R1 = 0.0624, wR2 = 0.1668	R1 = 0.1845, wR2 = 0.3789	R1 = 0.0394, wR2 = 0.1066
Largest diff. peak and hole (e·Å^{-3})	1.422 and -0.868	1.724 and -0.803	1.034 and -0.438

2. Powder X-ray diffraction (PXRD) analysis

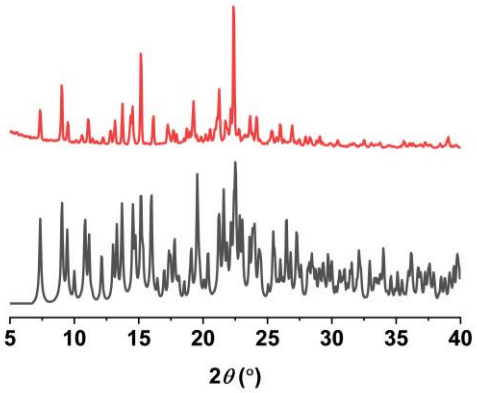

Fig. S2 PXRD patterns for simulated, as-synthesized 1D-DGIST-18 crystals after grinding.

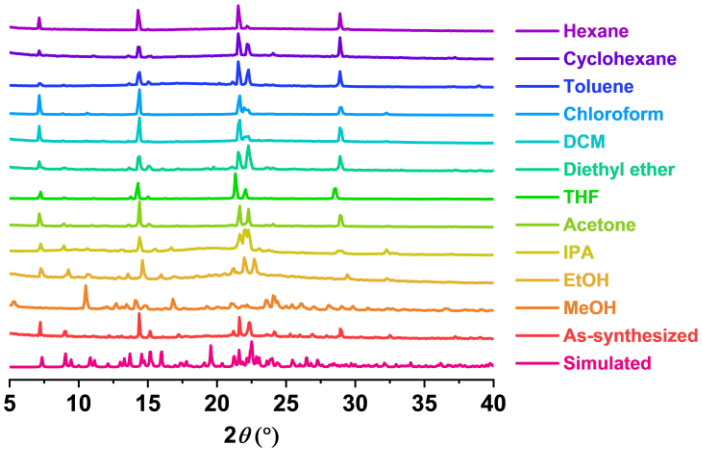

Fig. S3 PXRD patterns of simulated 1D-DGIST-18 and 1D-DGIST-18 samples after immersion in various solvents for a day.

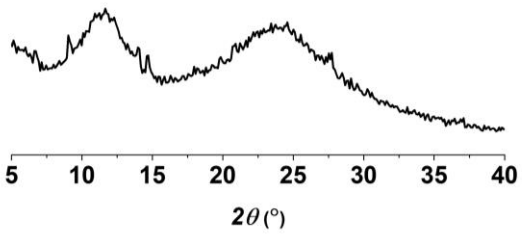

Fig. S4 PXRD pattern of 1D-acetone (2%)-DV.

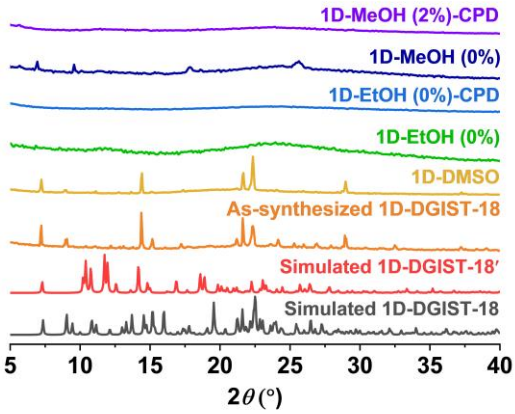

Fig. S5 PXRD patterns of simulated 1D-DGIST-18**,** simulated 1D-DGIST-18', as-synthesized 1D-DGIST-18, 1D-DMSO, 1D-EtOH (0%), 1D-EtOH (0%)-CPD, 1D-MeOH (0%), and 1D-MeOH (2%)-CPD.

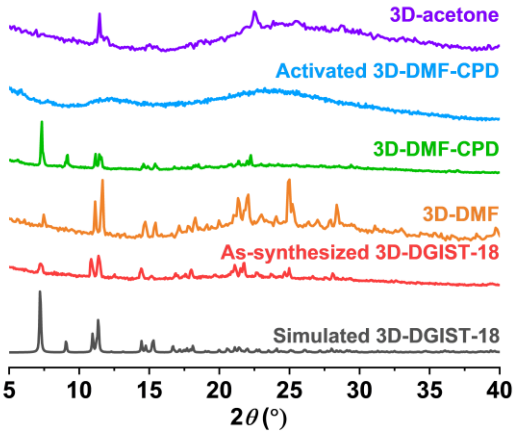

Fig. S6 PXRD patterns of simulated 3D-DGIST-18, as-synthesized 3D-DGIST-18, 3D-DMF, 3D-DMF-CPD, 3D-DMF-CPD, activated at 180 °C and 3D-acetone.

3. Gas sorption analysis of 1D-DGIST-18 and 3D-DGIST-18

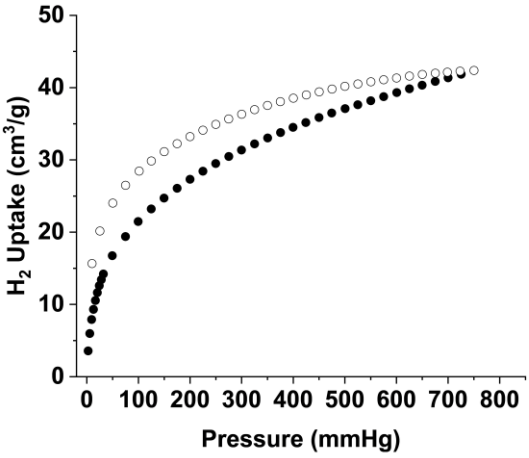

Fig. S7 H_2 adsorption–desorption isotherms of 1D-acetone (2%)-CPD at 77 K.

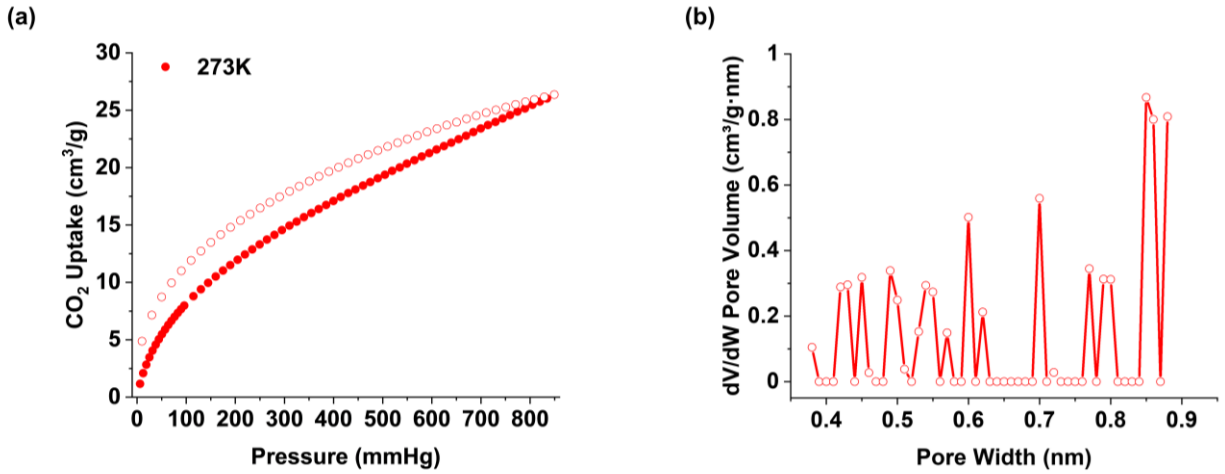

Fig. S8 (a) CO_2 adsorption–desorption isotherms at 273 K of 1D-acetone (2%)-CPD and (b) pore size distribution using the grand canonical Monte Carlo method.

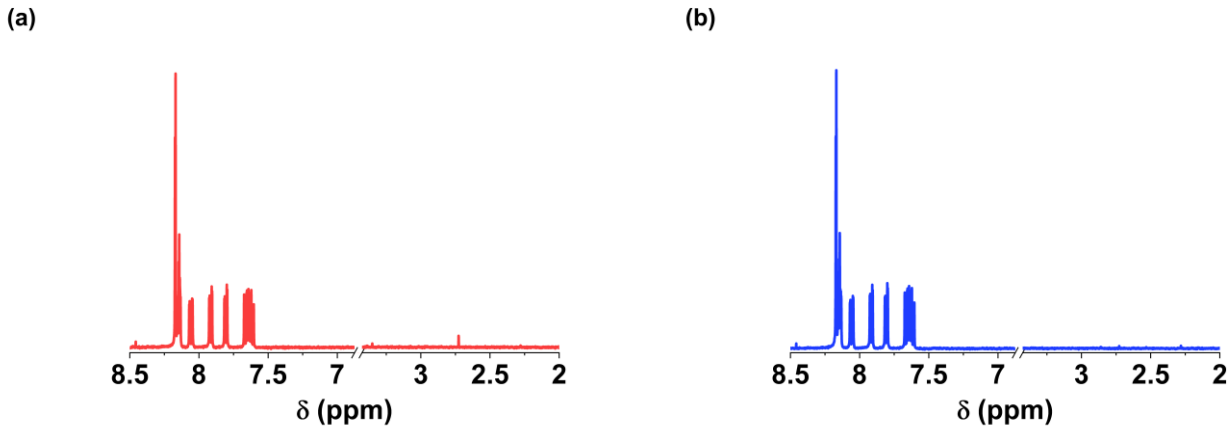

Fig. S9 ^{1}H-NMR spectra of (a) 1D-MeOH (0%) and (b) 1D-EtOH, after deprotonation using 0.1 M NaOH in D_2O.

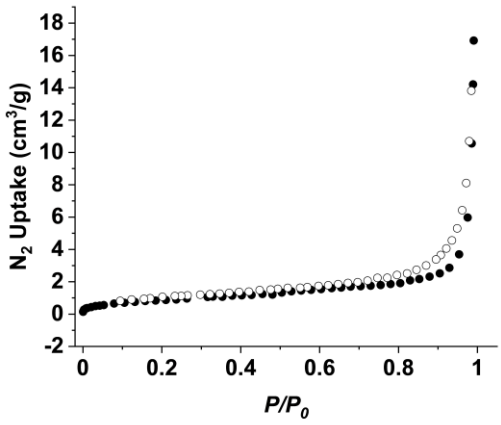

Fig. S10 N_2 adsorption–desorption isotherms at 77K of 1D-MeOH (0%)-CPD, activated at 80°C.

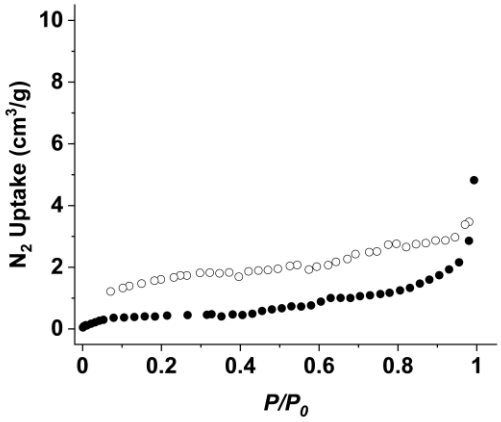

Fig. S11 N_2 adsorption–desorption isotherms at 77K of 3D-DMF-CPD, activated at 180 °C.

Table S2. 1D coordination polymers exhibiting gas sorption properties.

1D CP	Pore type	Surface area (m^2 g)				
		N_2	Ar	CO_2	O_2	Ref.
$[Mn(dhbq)(H_2O)_2]_n$	Micro	429 (BET, 77K)				8
$[Rh_2(bza)_4(pyz)]_n$	Micro	353 (BET, 77K)		274.1 (BET, 273K)	243.4 (BET, 77K)	9-11
$[Rh_2(bza)_4(1,5\text{-nptd})]_n$	Micro	292 (BET, 77K)				12
$[Zn(phen)(L1)]_n$	Micro	303 (Langmuir)				13
$[Zn(phen)(SDC)]_n$	Micro		220 (BET, 87K) 349 (Langmuir, 87K)			14
DDA-Cu	Micro, meso	127 (BET, 77K)				15
$[Cu(CF_3SO_3)_2(bpp)_2]_n$				1004 (Langmuir, 195K)		16
$[Cu(PF_6)_2(bpetha)_2]_n$		15 (BET, 77K)		882 (Langmuir, 195K)		17
$[Cu_2(bza)_4(2\text{-apyr})]_n$		15 (BET, 77K)		359 (BET, 195K)		18
$[Cu(2,2'\text{-bpy})(ipa)]_n \cdot 2nH_2O$		N/A		37 (BET, 195K)		19
$[(Ru_{(1-x)}Rh_x)_2(2,4,5\text{-}Me_3PhCO_2)_4(phz)]_n$				N/A		
$Cu(bpp)_2(BF_4)_2$		11 (BET, 77K)		N/A		20
$Ni(DBM)_2(bpy)$				N/A		21
$[Ru_2(p\text{-}MeOPhCO_2)_4(phz)]$				N/A		22
$[Zn(phen)_2L2]\cdot(3CH_3OH\cdot 6H_2O)$				N/A		23
$[Zn(ndc)(o\text{-phen})]\cdot DMF\}_n$				N/A		24
1D-DGIST-18	**Micro, Meso, Macro**	**243 (BET, 77K)**				**This work**

abbreviation

H_2dhbq = 2,5-dihydroxy-1,4-benzoquinon
bza = benzoate
pyz = pyrazine
1,5-nptd = 1,5-naphthyridine
H_2L1 = transstilbene-4,49-dicarboxylic acid
phen = 1,10-phenanthroline, H_2SDC = trans-4,40-stilbenedicarboxylic acid
DDA = 1,5-diamino-4,8-dihydroxy-9,10-anthraceneedione
bpp = 1,3-bis(4-pyridyl)propane
bpetha=1,2-bis(4-pyridyl)ethan
2-apyr = 2-aminopyrimidine
ipa = isophthalate, 2,2'-bpy =2,29-bipyridine
2,4,5-$Me_3PhCO_2^-$ = 2,4,5-trimethylbenzoate, phz = phenazine
DBM = dibenzylmethanate, bpy = 4,4′-bipyridine
p-$MeOPhCO_2^-$ = p-anisate
H_2L2 = 1-(4-carboxyphenyl)-5-mercapto-1H-tetrazol
o-phen=1,10-phenanthro-line, ndc=2,6-napthalenedicarboxylate

4. Field emission-scanning electron microscopy (FE-SEM)

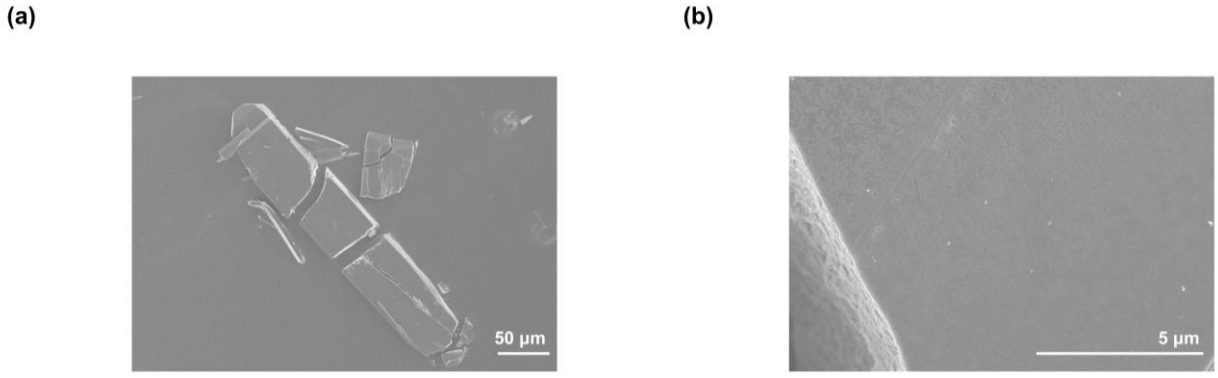

Fig. S12 FE-SEM images of 1D-acetone (2%)-CPD.

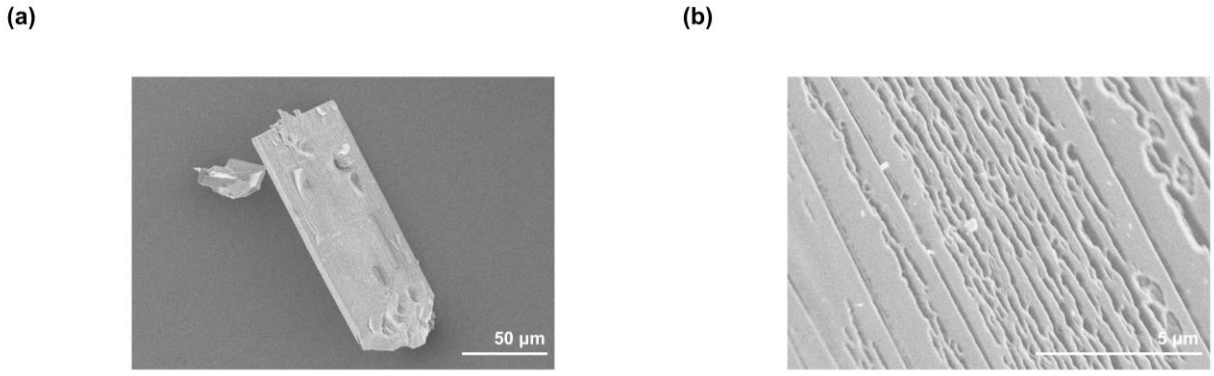

Fig. S13 FE-SEM images of 1D-MeOH (0%)-CPD.

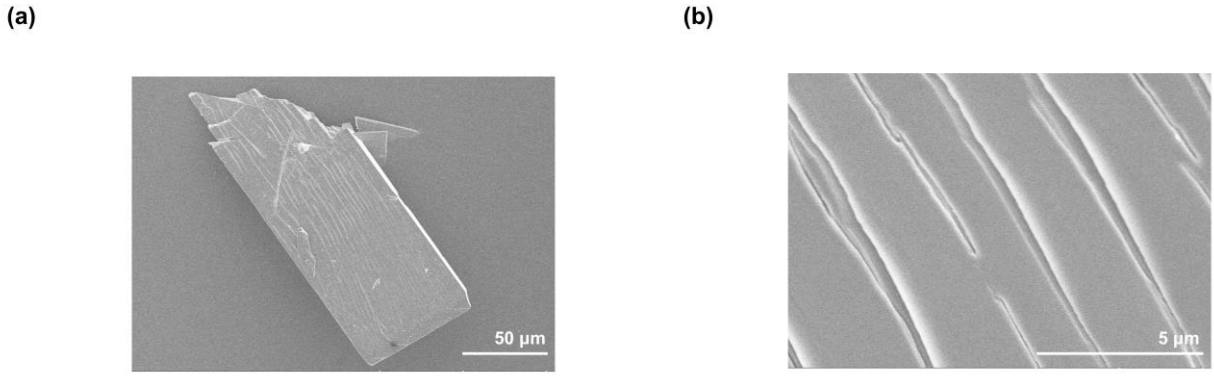

Fig. S14 FE-SEM images of 1D-EtOH (0%)-CPD.

5. Photoluminescence properties

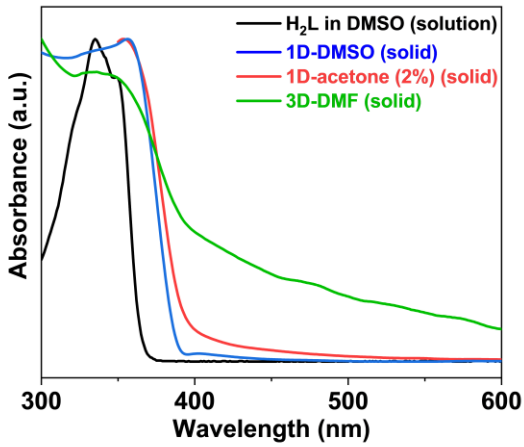

Fig. S15 UV-vis absorption spectra of H_2**L**, dissolved in DMSO (0.04 mM), 1D-DGIST-18 in DMSO and acetone, and 3D-DGIST-18 in DMF.

Table S3 Excitation (λex) and emission (λem) wavelength of filter set (unit: nm).

	Blue (DAPI)	Green (FITC)	Red (mCherry HQ)
λex	340-380	465-495	550-590
λem	435-485	515-555	608-683

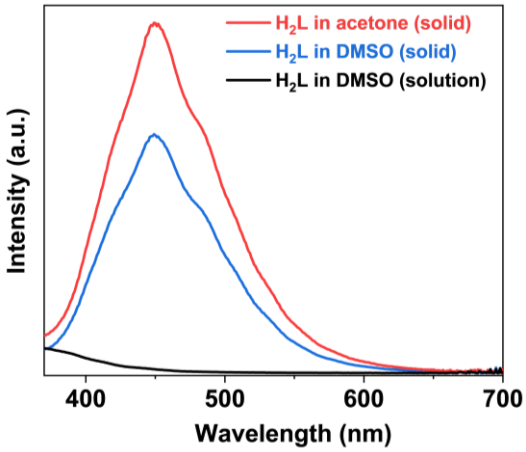

Fig. S16 Emission spectra of H_2**L**, dissolved in DMSO (13.8 mM), and H_2**L,** soaked in DMSO and acetone.

Stretched exponential decay function for the TCSPC interpretation. β_1 is the stretching exponent.

$$y = A_1 * \exp\left(-\left(\frac{x}{t_1}\right)^{\beta}\right) + A_2 * \exp\left(-\left(\frac{x}{t_2}\right)\right) + y_0 \quad \text{(Eq. S1)}$$

6. Thermogravimetric analysis (TGA)

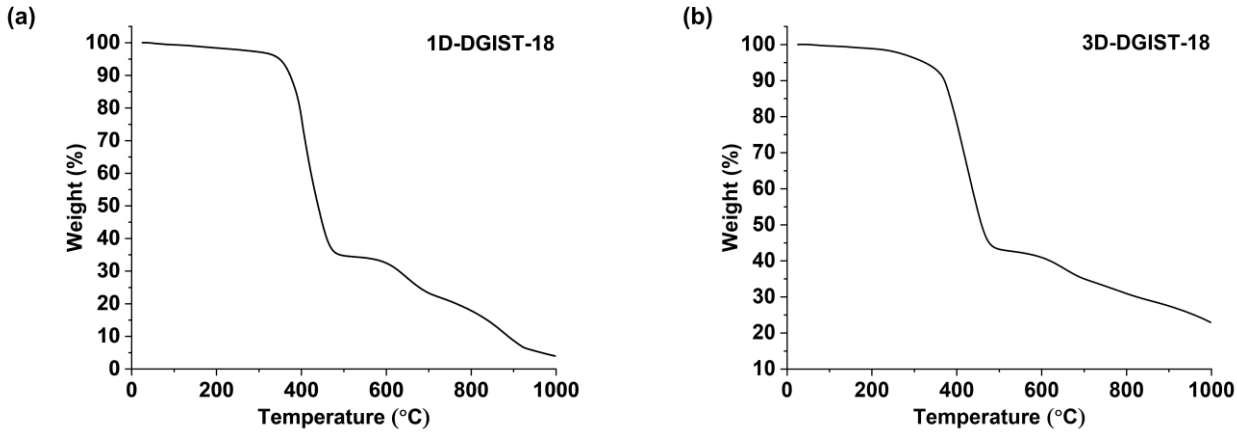

Fig. S17 TGA curves for (a) 1D-DGIST-18 and (b) 3D-DGIST-18. Evacuated (a) 1D-DGIST-18 and (b) 3D-DGIST-18 demonstrated stability up to 376 and 363 °C, respectively.

References

1 K. Jin, X.-Q. Wu, Y.-P. Chen, I.-H. Park, J.-R. Li and J. Park, *Inorg. Chem.*, 2022, **61**, 1918-1927.
2 Y. Keum, B. Kim, A. Byun and J. Park, *Angew. Chem. Int. Ed.*, 2020, **59**, 21591-21596.
3 J. W. Shin, K. Eom and D. Moon, *J. Synchrotron Rad.*, 2016, **23**, 369-373.
4 Z. Otwinowski and W. Minor, in *Methods in Enzymology*, Academic Press, 1997, vol. 276, pp. 307-326.
5 G. Sheldrick, *Acta Cryst.*, 2015, **A71**, 3-8.
6 G. Sheldrick, *Acta Cryst.*, 2015, **C71**, 3-8.
7 A. L. Spek, *Acta Cryst.*, 2015, **71**, 9-18.
8 L. Li, L. Guo, D. H. Olson, S. Xian, Z. Zhang, Q. Yang, K. Wu, Y. Yang, Z. Bao, Q. Ren and J. Li, *Science*, 2022, **377**, 335-339.
9 S. Takamizawa, T. Hiroki, E.-i. Nakata, K. Mochizuki and W. Mori, *Chem. Lett.*, 2002, **31**, 1208-1209.
10 S. Takamizawa, E.-i. Nakata and T. Saito, *CrystEngComm*, 2004, **6**, 39-41.
11 S. Takamizawa, E.-i. Nakata, H. Yokoyama, K. Mochizuki and W. Mori, *Angew. Chem. Int. Ed.*, 2003, **42**, 4331-4334.
12 S. Takamizawa, E.-i. Nakata and T. Saito, *Inorg. Chem. Commun.*, 2004, **7**, 125-127.
13 A.-L. Cheng, N. Liu, Y.-F. Yue, Y.-W. Jiang, E.-Q. Gao, C.-H. Yan and M.-Y. He, *Chem. Comm.*, 2007, 407-409.
14 G. K. Kole, A. J. Cairns, M. Eddaoudi and J. J. Vittal, *New J. Chem.*, 2010, **34**, 2392-2395.
15 S. Shang, C. Du, Y. Liu, M. Liu, X. Wang, W. Gao, Y. Zou, J. Dong, Y. Liu and J. Chen, *Nat. Commun.*, 2022, **13**, 7599.
16 K. Fukuhara, S.-i. Noro, K. Sugimoto, T. Akutagawa, K. Kubo and T. Nakamura, *Inorg. Chem.*, 2013, **52**, 4229-4237.
17 S.-i. Noro, D. Tanaka, H. Sakamoto, S. Shimomura, S. Kitagawa, S. Takeda, K. Uemura, H. Kita, T. Akutagawa and T. Nakamura, *Chem. Mater.*, 2009, **21**, 3346-3355.
18 S.-i. Noro, Y. Meng, K. Suzuki, M. Sugiura, Y. Hijikata, J. Pirillo, X. Zheng, K. Takahashi and T. Nakamura, *Inorg. Chem.*, 2021, **60**, 4531-4538.
19 L. Li, J. Yang, Q. Zhao and J. Li, *CrystEngComm*, 2013, **15**, 1689-1692.
20 R. Kotani, A. Kondo and K. Maeda, *Chem. Comm.*, 2012, **48**, 11316-11318.
21 J. T. Culp, A. L. Goodman, D. Chirdon, S. G. Sankar and C. Matranga, *J. Phys. Chem. C*, 2010, **114**, 2184-2191.
22 W. Kosaka, J. Zhang, Y. Watanabe and H. Miyasaka, *Inorg. Chem.*, 2022, **61**, 12698-12707.
23 J.-H. Deng, J. Luo, Y.-L. Mao, S. Lai, Y.-N. Gong, D.-C. Zhong and T.-B. Lu, *Sci. Adv.*, 2020, **6**, eaax9976.
24 R. Haldar, R. Matsuda, S. Kitagawa, S. J. George and T. K. Maji, *Angew. Chem. Int. Ed.*, 2014, **53**, 11772-11777.